Rapid Communications

Phase transition preceding magnetic long-range order in the double perovskite Ba_2NaOsO_6

Kristin Willa,[1,2] Roland Willa,[1,3] Ulrich Welp,[1] Ian R. Fisher,[4,5] Andreas Rydh,[6] Wai-Kwong Kwok,[1] and Zahir Islam[7]

[1]*Materials Science Division, Argonne National Laboratory, 9700 South Cass Avenue, Argonne, Illinois 60439, USA*

[2]*Institute for Solid State Physics, Karlsruhe Institute of Technology, D-76021 Karlsruhe, Germany*

[3]*Institute for Theory of Condensed Matter, Karlsruhe Institute of Technology, D-76131 Karlsruhe, Germany*

[4]*Department of Applied Physics and Geballe Laboratory for Advanced Materials, Stanford University, Stanford, California 94305, USA*

[5]*Stanford Institute for Materials and Energy Sciences, SLAC National Accelerator Laboratory, 2575 Sand Hill Road, Menlo Park, California 94025, USA*

[6]*Department of Physics, Stockholm University, SE-106-91 Stockholm, Sweden*

[7]*Advanced Photon Source, Argonne National Laboratory, 9700 South Cass Avenue, Argonne, Illinois 60439, USA*

(Received 9 May 2019; published 15 July 2019)

Recent theoretical studies [G. Chen *et al.*, Phys. Rev. B **82**, 174440 (2010); H. Ishizuka *et al.*, Phys. Rev. B **90**, 184422 (2014)] for the magnetic Mott insulator Ba_2NaOsO_6 have proposed a low-temperature order parameter that breaks lattice rotational symmetry without breaking time reversal symmetry, leading to a nematic phase just above the magnetic ordering temperature. We present high-resolution calorimetric and magnetization data of the same Ba_2NaOsO_6 single crystal and show evidence for a weakly field-dependent phase transition occurring at a temperature of $T_s \approx 9.5$ K, above the magnetic ordering temperature of $T_c \approx 7.5$ K. This transition appears as a broadened step in the low-field temperature dependence of the specific heat. The evolution of the phase boundary with applied magnetic field suggests that this phase coincides with the phase of broken local point symmetry seen in NMR experiments at high fields [L. Lu *et al.*, Nat. Commun. **8**, 14407 (2017)]. Furthermore, the magnetic field dependence of the specific heat provides clear indications for magnetic correlations persisting at temperatures between T_c and T_s where long-range magnetic order is absent, giving support for the existence of the proposed nematic phase.

DOI: 10.1103/PhysRevB.100.041108

The simultaneous occurrence of strong spin-orbit coupling (SOC), orbital degrees of freedom, and electronic correlations gives rise to a remarkable variety of electronic states [1,2] ranging from unconventional superconducting and magnetic phases to spin liquids and topological states of matter. This richness is on display in the rocksalt ordered double perovskites with a general composition $A_2BB'O_6$ [3,4], where B denotes a nonmagnetic ion and B' an ion with partially filled $4d$ or $5d$ orbitals. The double perovskite structure can be viewed as two interpenetrating fcc lattices of O octahedra centered around the B and B' ions, respectively, resulting in a geometrically frustrated arrangement of magnetic moments with a relatively large separation. Consequently, the magnetic exchange, spin-orbit coupling, and correlation energies are of comparable magnitude such that a diverse range of ground states can arise. In particular, the strong SOC induces highly anisotropic non-Heisenberg exchange interactions [5] which depend on the orbital occupancy and are therefore strongly tied to orbital order [6–15].

Among these double perovskites, the Mott-insulating Ba_2NaOsO_6 has garnered particular interest as it undergoes a ferromagnetic transition below 8 K [16–18] with a (110) easy axis [17] that is not expected in standard Landau theory of magnetic anisotropy for a cubic system [8] and a negative Curie-Weiss temperature indicative of antiferromagnetism [17]. The formal valence of Os is 7^+ corresponding to a $5d^1$ state, although hybridization between Os-$5d$ and O-$2p$ states has been recognized as an important factor determining the magnetic state of Os [10,13] and may be responsible for the small saturation moment $\leqslant 0.2\mu_B$/Os. The $5d^1$ configuration in an octahedral crystal field in the presence of strong SOC leads to a fourfold degenerate t_{2g} ground state corresponding to an effective angular momentum of $3/2$. This state is unstable against a Jahn-Teller distortion [10,11,15] that induces a tetragonal paramagnetic phase with a twofold degenerate ground state, as also indicated by measurements of the entropy balance across the magnetic transition yielding a value close to $R \ln 2$ [17] rather than $R \ln 4$ as seen in a recent study on the related compound Ba_2MgReO_6 [19]. Furthermore, recent high-field NMR experiments [20,21] reveal that the magnetically ordered state of Ba_2NaOsO_6 is composed of an exotic noncollinear magnetic structure in which successive ferromagnetic Os-Na layers subtend a canting angle of $\approx 134^\circ$ resulting in a small net magnetic moment along (110). This long-range magnetic order is driven by orbital ordering and has an overall orthorhombic symmetry. In addition, at high magnetic fields and several degrees Kelvin above the magnetic transition temperature, signatures of orbital ordering into a state that preserves time reversal symmetry but breaks the fourfold lattice symmetry of the high-temperature paramagnetic phase have been reported [20,21]. However, the evolution of this phase at low fields has not been reported so far.

Here we draw a holistic thermodynamic picture of Ba_2NaOsO_6 by presenting calorimetric data and magnetization data obtained from the same single crystal. Using general thermodynamic considerations and the Fisher

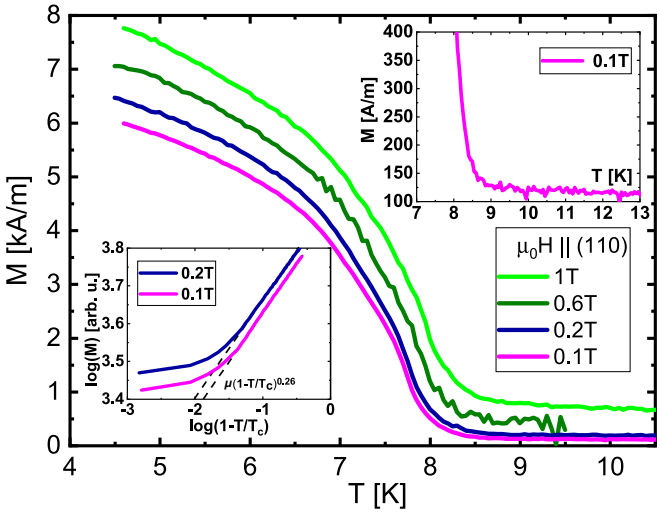

FIG. 1. Temperature-dependent magnetization for a Ba_2NaOsO_6 single crystal in various fields applied along (110). Approaching the transition temperature from below, the magnetization vanishes as $M \propto (1 - T/T_c)^{\eta}$, with $\eta \approx 0.26$ and $T_c = 7.5$ K (bottom inset). The top inset shows the magnetization on largely expanded scales and highlights that the tail of the magnetic transition extends to beyond 9 K.

formula [22], we separate magnetic and nonmagnetic contributions to the specific heat, and present evidence for a largely field-independent phase transition occurring at $T_s \approx 9.5$ K, slightly above the magnetic ordering temperature of $T_c \approx 7.5$ K. This transition appears as a broadened step in the temperature dependence of the specific heat, and its evolution with applied magnetic field suggests that this phase corresponds to the broken local point symmetry phase seen at NMR experiments in high fields [20,21]. Our specific heat results, in conjunction with the NMR findings, indicate that this phase between T_c and T_s is nematic in origin, as predicted by theoretical models [8,11]. Here, we establish its low-field phase boundary. The magnetic field dependence of the specific heat reveals that magnetic correlations persist into the nematic phase even though long-range magnetic order is absent.

Single crystals of Ba_2NaOsO_6 were grown by molten hydroxide flux, following the method presented in Ref. [16]. We polished a platelike sample perpendicular to the (001) direction down to approximately 34 μm thickness. The crystal was then successively attached with its polished surface onto a quartz fiber for superconducting quantum interference device (SQUID) magnetometry and onto a nanocalorimetric membrane for specific heat measurements. In both setups, the external magnetic field was applied along the crystallographic (110) direction, the magnetic easy axis [17]. The magnetization data reveal the onset of magnetic order at temperatures below 8 K, as evidenced by the steep increase in the magnetization (see Fig. 1), in agreement with earlier reports [16–18]. Over a remarkably wide temperature range, the magnetization follows the relation $M(T) \approx (1 - T/T_c)^{\eta}$ with $\eta \approx 0.26$ (see Fig. 1). Determining the magnetic transition temperature $T_c = 7.4$ K from this scaling is in good agreement with the calorimetric results presented below.

Specific heat data were obtained using a membrane-based ac calorimeter as described in Refs. [23,24] and pictured in the inset of Fig. 3. Through the membrane's ac heater, the sample is subjected to a modulated heat signal, and the resulting temperature oscillation is recorded as a second harmonic tone. Along a temperature scan, the oscillation frequency is kept constant (around 1 Hz) and the heater power is adjusted to keep a constant relation between the absolute temperature and temperature modulation amplitude. The specific heat data in zero applied field and in fields up to 6 T are shown in Fig. 2(b). In zero field, we observe a sharp central peak at 7.5 K that signals the transition into the magnetically ordered state which is accompanied by a small shoulder on the high-temperature side, consistent with an earlier zero-field specific heat study [17]. Additionally a low-temperature shoulder can be seen which, for increasing fields, moves, together with the main peak, to higher temperatures (at a rate of 0.26 K/T) until they merge in high fields. This is indicative for both features being magnetic in origin, albeit the causes of the shoulder are not known at present. On the contrary, the high-temperature shoulder does not depend on field strength for small fields. Interpreting this shoulder as a broadened step centered near 9.5 K, we estimate the associated step height of 50 mJ/mol K^2. At fields higher than 1.5 T, this shoulder is masked by the main peak moving to higher temperatures. However, as revealed by the temperature derivative of the 4- and 6-T data, signatures of the shoulder are still discernible in high applied fields residing on the high-temperature slope of the main peak, as marked by the arrows in Fig. 2(c). At 4 T, the sharp dip at 9 K originates from the main inflection point of the C/T curve, while the feature due to the shoulder occurs near 9.7 K (see arrow). In 6 T, the inflection point is shifted to ≈ 9.8 K and the shoulder to 10.3 K. For reference, the 0-T data have been included.

In order to gain further insight into the origin of the calorimetric response, we apply the Fisher relation [22],

$$C(T) \simeq A\{\partial[T\chi(T)]/\partial T\}, \tag{1}$$

which links the magnetic specific heat C_m associated with an antiferromagnetic transition to the temperature dependence of the zero-field susceptibility $\chi = (\partial M/\partial H)|_{H=0}$. Here, the parameter A depends only weakly on temperature. This relation has been applied extensively to the investigation of antiferromagnetic transitions, for instance, in dysprosium aluminum garnet [25], $HoAsO_4$ and $GdVO_4$ [26,27], and more recently in Fe-based superconductors [27–29]. The work on the Fe-based superconductors, in particular, revealed that Eq. (1) yields a good description of magnetization and caloric data also at temperatures beyond the vicinity of the antiferromagnetic transition. Nevertheless, its applicability to Ba_2NaOsO_6 may be questioned since this material is not a simple antiferromagnet but rather dominated by the ferromagnetic component. On the other hand the large canting angle between ferromagnetic layers induces predominantly antiferromagnetic correlations, as evidenced, for instance, by the negative Curie-Weiss temperature [$\Theta = -13$ K for $H||(110)$] and by a comparatively small ferromagnetic moment of less than $0.2\mu_B$/Os [17]. We therefore contend that relation (1) is suitable for analyzing the magnetic and caloric properties of this material. We apply Eq. (1) to the

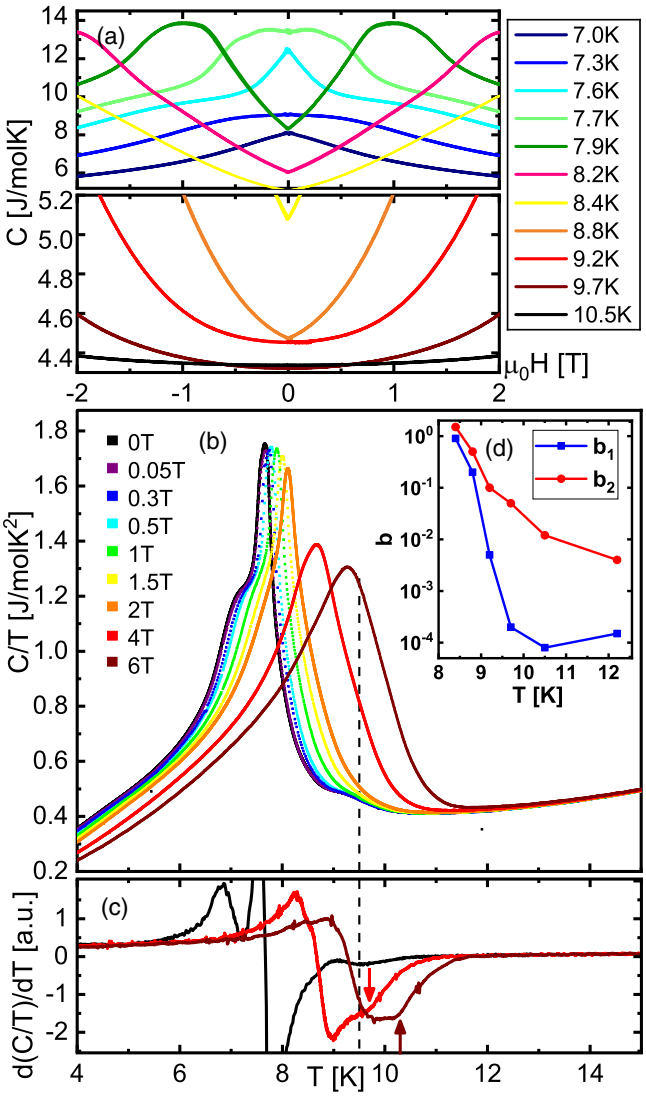

FIG. 2. (a) Isothermal magnetic field dependence of the specific heat of a Ba_2NaOsO_6 single crystal. (b) Temperature dependence of the specific heat of a Ba_2NaOsO_6 single crystal at fixed magnetic fields along the (110) direction. The main peak corresponds to the magnetic phase transition, while we attribute the high-temperature shoulder near 9.5 K (indicated by the dotted line) to a nematic transition. No field dependence is observed for the nematic transition up to 0.5 T. For higher fields, this transition is masked by the main magnetic transition. (c) Temperature derivative of the specific heat data at 0, 4, and 6 T. The shoulder feature in C/T corresponds to a negative-going dip in the derivative, as seen in the 0-T trace at the location of the dashed line. In fields of 4 and 6 T this dip has shifted to 9.7 and 10.3 K, respectively, as marked by the arrows revealing the nematic transition. (d) Temperature dependence of the parameters b_1 and b_2 entering the fit $C(H,T) = C_0(T) + b_1(T)\mu_0|H| + b_2(T)(\mu_0 H)^2 + b_4(T)(\mu_0 H)^4$.

magnetization data taken in a field of 0.1 T and approximate the susceptibility as $\chi = M/H$. From the measured specific heat we subtracted a background ($C_{\text{backgd}} = \alpha' T + \alpha T^3$). As shown in Fig. 3, the peak position and shape as well as the low-temperature shoulder are well reproduced. However, the high-temperature shoulder is absent in the specific heat

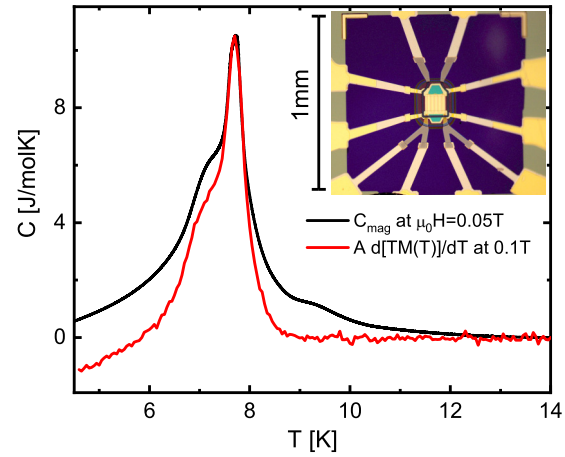

FIG. 3. Comparison of $A\partial[TM(T)]/\partial T$ evaluated in a field of 0.1 T (red) and the measured specific heat after subtracting a phonon background (black). A moving average of five points has been applied to the magnetization data prior to taking the derivative. Here, the coefficient A has been adjusted to match the peak heights. The location and shape of the main magnetic peak and the low-temperature shoulder are well reproduced. However, the high-temperature shoulder near 9.5 K is absent in the data derived from the magnetization, suggesting that this feature is largely nonmagnetic in origin. The nanocalorimeter platform is shown in the inset.

curve derived from the magnetization data, suggesting that this feature is largely nonmagnetic, possibly structural, in origin and does not change the magnetic level degeneracy. In combination with the results from Ref. [17], this points to a scenario of a transition at T_s between noncubic states. Shoulders in the specific heat preceding a magnetic transition similar to those observed here have been reported in studies of the phase transitions of $Ba(Fe_{1-x}Co_x)_2As_2$, where they were attributed to a second-order structural transition between the high-temperature tetragonal paramagnetic phase and an orthorhombic nematic phase [28,29]. The magnetization of $Ba(Fe_{1-x}Co_x)_2As_2$ does display a change in slope at the structural transition such that the application of Eq. (1) yields the shoulder in the specific heat, in contrast to the data presented here on Ba_2NaOsO_6. This behavior of $Ba(Fe_{1-x}Co_x)_2As_2$ has been ascribed to the pronounced magnetoelastic coupling reported in Fe-based superconductors [30–32]. While theoretical considerations [10,11,14] indicate strong magnetoelastic coupling for Ba_2NaOsO_6, our results imply that this coupling is weaker than in Fe-based superconductors.

The good agreement between the specific heat measured directly and that derived from magnetization data using the Fisher relation (1) allowed us to qualitatively disentangle magnetic from nonmagnetic calorimetric contributions. We reach beyond this approach by performing detailed measurements of the field dependence of the specific heat and analyzing the data according to the thermodynamic relation [33]

$$\partial C/\partial B = T(\partial^2 M/\partial T^2), \tag{2}$$

derived from the Gibbs free energy $G(T,H) = U - ST + pV - MH$. The upper panel of Fig. 2 shows the field dependence of the specific heat measured at temperatures

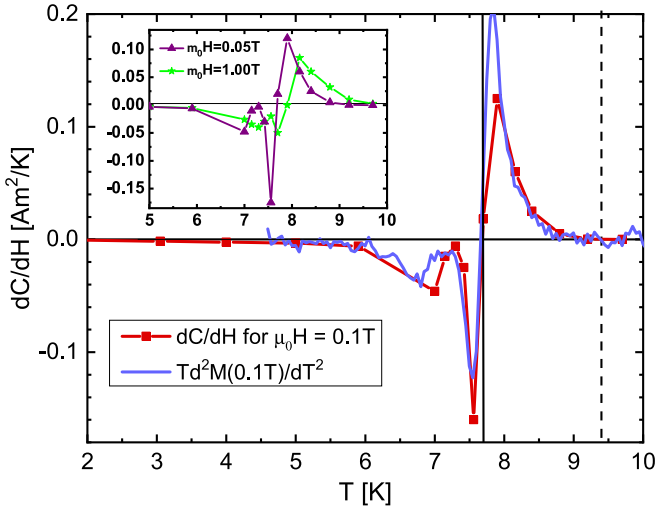

FIG. 4. The thermodynamic relation (2) is tested here by plotting the derivatives $\partial C/\partial H$ (red) and $T\partial^2 M/\partial T^2$ (blue) against temperature and for a fixed field of 0.1 T. The absence of a feature above 7.5 K is evidence for the structural origin of the high-temperature shoulder observed in the specific heat (see Fig. 2). The inset shows $\partial C/\partial H$ for two other fields, 0.05 and 1 T, allowing us to track the field dependence of the low-temperature shoulder and peak position (zero crossing) of the specific heat.

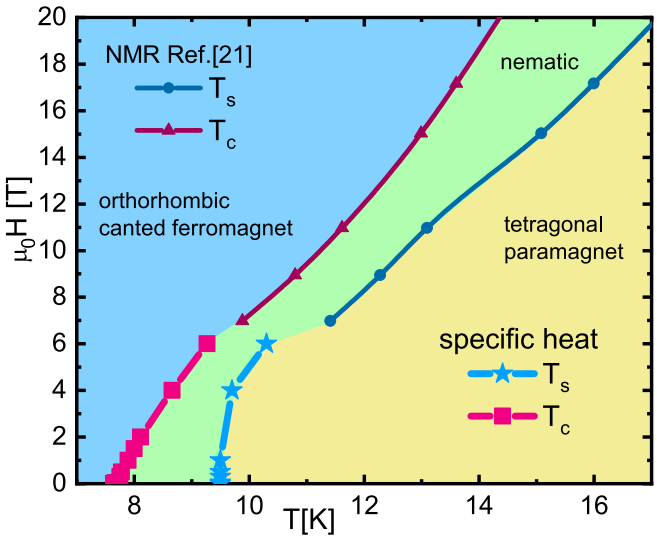

FIG. 5. Magnetic phase diagram of Ba_2NaOsO_6 as deduced from specific heat measurements containing the orthorhombic canted ferromagnetic phase at low temperatures, the nematic (i.e., orthorhombic paramagnetic) phase at intermediate temperatures, and the tetragonal paramagnetic phase at high temperatures. Shown are the fields of the peak in the specific heat marking the transition to long-range magnetic order (magenta) and the high-temperature shoulder (light blue) marking the beginning of the nematic phase. Also included are the high-field data from NMR experiments [21] for the magnetic transition (purple) and nematic phase (phase of broken local point symmetry) (dark blue). NMR data were taken in fields applied along a (001) direction while the specific heat was measured in (110) fields.

near the zero-field magnetic transition. Its nonmonotonic field dependence clearly reflects the shift of the magnetic transition to higher temperatures in increasing field. Above the magnetic transition and in the field range of $|\mu_0 H| < 1$ T, the specific heat can be well parametrized by $C(H,T) = C_0(T) + b_1(T)\mu_0|H| + b_2(T)(\mu_0 H)^2 + b_4(T)(\mu_0 H)^4$. The $|H|$ term accounts for the cusplike variation seen at temperatures below 9.5 K. The (in leading order) quadratic dependence in the high-temperature phase implies that in the limit of small fields, the specific heat is indeed field independent. More quantitatively, the linear coefficient b_1 at 9.5 K, disappears rapidly as compared to the quadratic coefficient b_2, see Fig. 2(d). While b_1 falls to zero within our experimental resolution $\sim 10^{-4}$, b_4 drops from $b_4 \approx 0.05$ at 9.2 K to values of 4×10^{-4} at 10.5 K as well, leaving the quadratic coefficient b_2 as the leading-order term. A quadratic field dependence of the specific heat, such as observed above 9.5 K, is expected for a system with field-independent susceptibility $M(T,H) = \chi(T)H$. In this case, Eq. (2) can be integrated to yield $C(H,T) = C_0(T) + (1/2)\mu_0 T H^2 \partial^2 \chi(T)/\partial T^2$. Thus, the salient feature of the data in Fig. 2(d) is that at low applied fields a nonlinear susceptibility and magnetic correlations emerge when cooling below 9.5 K. Within our resolution, these features remain unresolved in the magnetization (inset in Fig. 1). Compared with a simple Curie-Weiss law, the quadratic coefficient b_2 in the specific heat drops much faster, which is consistent with strong deviations of the susceptibility from a Curie-Weiss behavior below 20 K reported elsewhere [17].

Equation (2) can be used to validate the experimental data. As shown in Fig. 4, the second derivative of the magnetization (obtained from Fig. 1) is in excellent quantitative agreement with the first derivative of the specific heat (data from Fig. 2). The calibration-free agreement underlines the consistency across the different measurements while the absence of any features above 9.5 K (marked by the dotted line) confirms again the nonmagnetic origin of the high-temperature shoulder.

We use the specific heat data from Figs. 2 and 4 to construct the phase diagram as displayed in Fig. 5. Shown are the fields of the peak in the specific heat (respectively the zero crossing in $\partial C/\partial H$) marking the transition to long-range magnetic order and the high-temperature shoulder. Also included are the high-field data from NMR experiments for the magnetic transition and the transition to a phase of broken local point symmetry [21]. The evolution of the latter boundary with applied magnetic field suggests that the high-temperature shoulder represents the continuation of the broken local point symmetry phase to low fields. As this transition involves the distortion of oxygen octahedra and is thus primarily structural in origin, an almost field-independent transition may be expected at low fields. At the same time, the entanglement of spin, orbital, and lattice degrees of freedom inherent to the Mott-insulating double perovskites may account for the emergence of correlation effects and the field dependence of the specific heat, in particular, in fields above 4 T. Indeed, recent *ab initio* calculations [14] indicate that, due to this entanglement, the lattice vibrations and atomic positions become dependent on an effective magnetic field which contains contributions from an exchange field arising from magnetic correlations and from the applied field. The shape of the phase boundary suggests that this exchange corresponds to

an internal field scale of approximately 4 T, as in applied fields higher than this crossover field the phase boundary is clearly field dependent. While the inflection point in the phase boundary from the ferromagnetic to the nematic state might be an artifact from linking the two different data sets (NMR and specific heat), it coincides with the disappearance of the paramagnetic phase at 9 K. This as well can be seen as an internal scale of the paramagnetic interactions which have to be overcome in order to allow for an expansion of the orthorhombic ferromagnetic phase.

In conclusion, we have presented high-resolution calorimetric and magnetization data obtained on the same Ba_2NaOsO_6 single crystal. By differentiating magnetic and nonmagnetic contributions, we find at low fields a largely field-independent phase transition occurring a few degrees Kelvin above the magnetic transition. At higher fields this transition becomes field dependent, and the thus obtained phase boundary agrees well with a recent high-field NMR study that reports a phase of broken local point symmetry above the magnetic ordering temperature. Our results imply that the transition into the nematic state is indeed a thermodynamic phase transition. Furthermore, the magnetic field dependence of the specific heat gives a clear indication that magnetic correlations persist in the nematic phase $T_s > T > T_c$ even though long-range magnetic order is absent.

We thank Han-Oh Lee for help with crystal growth and Paul Wiecki as well as Frederic Hardy and Christoph Meingast for useful discussions. This work was supported by the U.S. Department of Energy, Office of Science, Basic Energy Sciences, Materials Sciences and Engineering Division. Both K. W. and R.W. acknowledge support from the Swiss National Science Foundation through the Early Postdoc. Mobility program. Work at Stanford University was supported by the DOE, Office of Basic Energy Sciences, under Contract No. DE-AC02-76SF00515. This research used resources of the Advanced Photon Source, a U.S. Department of Energy (DOE) Office of Science User Facility operated for the DOE Office of Science by Argonne National Laboratory under Contract No. DE-AC02-06CH11357.

[1] W. Witczak-Krempa, G. Chen, Y. B. Kim, and L. Balents, Ann. Rev. Condens. Matter Phys. **5**, 57 (2014).
[2] J. G. Rau, E. K.-H. Lee, and H.-Y. Kee, Annu. Rev. Condens. Matter Phys. **7**, 195 (2016).
[3] S. Vasala and M. Karppinen, Prog. Solid State Chem. **43**, 1 (2015).
[4] C. A. Marjerrison, C. M. Thompson, G. Sala, D. D. Maharaj, E. Kermarrec, Y. Cai, A. M. Hallas, M. N. Wilson, T. J. S. Munsie, G. E. Granroth, R. Flacau, J. E. Greedan, B. D. Gaulin, and G. M. Luke, Inorg. Chem. **55**, 10701 (2016).
[5] K. I. Kugel' and D. I. Khomskiĭ, Sov. Phys. Usp. **25**, 231 (1982).
[6] H. J. Xiang and M.-H. Whangbo, Phys. Rev. B **75**, 052407 (2007).
[7] S. Gangopadhyay and W. E. Pickett, Phys. Rev. B **91**, 045133 (2015).
[8] G. Chen, R. Pereira, and L. Balents, Phys. Rev. B **82**, 174440 (2010).
[9] C. Svoboda, M. Randeria, and N. Trivedi, arXiv:1702.03199.
[10] L. Xu, N. Bogdanov, A. Princep, P. Fulde, J. van den Brink, and L. Hozoi, npj Quantum Mater. **1**, 16029 (2016).
[11] H. Ishizuka and L. Balents, Phys. Rev. B **90**, 184422 (2014).
[12] J. Romhányi, L. Balents, and G. Jackeli, Phys. Rev. Lett. **118**, 217202 (2017).
[13] K.-H. Ahn, K. Pajskr, K.-W. Lee, and J. Kuneš, Phys. Rev. B **95**, 064416 (2017).
[14] N. Iwahara, V. Vieru, and L. F. Chibotaru, Phys. Rev. B **98**, 075138 (2018).
[15] T. Dodds, T.-P. Choy, and Y. B. Kim, Phys. Rev. B **84**, 104439 (2011).
[16] K. E. Stitzer, M. D. Smith, and H.-C. zur Loye, Solid State Sci. **4**, 311 (2002).
[17] A. S. Erickson, S. Misra, G. J. Miller, R. R. Gupta, Z. Schlesinger, W. A. Harrison, J. M. Kim, and I. R. Fisher, Phys. Rev. Lett. **99**, 016404 (2007).
[18] A. J. Steele, P. J. Baker, T. Lancaster, F. L. Pratt, I. Franke, S. Ghannadzadeh, P. A. Goddard, W. Hayes, D. Prabhakaran, and S. J. Blundell, Phys. Rev. B **84**, 144416 (2011).
[19] D. Hirai and Z. Hiroi, J. Phys. Soc. Jpn. **88**, 064712 (2019).
[20] L. Lu, M. Song, W. Liu, A. P. Reyes, P. Kuhns, H. O. Lee, I. R. Fisher, and V. F. Mitrović, Nat. Commun. **8**, 14407 (2017).
[21] W. Liu, R. Cong, E. Garcia, A. Reyes, H. Lee, I. Fisher, and V. Mitrović, Physica B: Condens. Matter **536**, 863 (2018).
[22] M. E. Fisher, Philos. Mag. **7**, 1731 (1962).
[23] K. Willa, Z. Diao, D. Campanini, U. Welp, R. Divan, M. Hudl, Z. Islam, W.-K. Kwok, and A. Rydh, Rev. Sci. Instrum. **88**, 125108 (2017).
[24] S. Tagliati, V. M. Krasnov, and A. Rydh, Rev. Sci. Instrum. **83**, 055107 (2012).
[25] W. P. Wolf and A. F. G. Wyatt, Phys. Rev. Lett. **13**, 368 (1964).
[26] W. Becher, H. Kalbfleisch, and K. Melchior, Physica B+C **80**, 215 (1975).
[27] N. Ni, M. E. Tillman, J.-Q. Yan, A. Kracher, S. T. Hannahs, S. L. Bud'ko, and P. C. Canfield, Phys. Rev. B **78**, 214515 (2008).
[28] J.-H. Chu, J. G. Analytis, C. Kucharczyk, and I. R. Fisher, Phys. Rev. B **79**, 014506 (2009).
[29] C. R. Rotundu and R. J. Birgeneau, Phys. Rev. B **84**, 092501 (2011).
[30] H.-H. Kuo, J. G. Analytis, J.-H. Chu, R. M. Fernandes, J. Schmalian, and I. R. Fisher, Phys. Rev. B **86**, 134507 (2012).
[31] R. M. Fernandes, A. V. Chubukov, and J. Schmalian, Nat. Phys. **10**, 97 (2014).
[32] R. M. Fernandes, A. E. Böhmer, C. Meingast, and J. Schmalian, Phys. Rev. Lett. **111**, 137001 (2013).
[33] H. E. Stanley, *Phase Transitions and Critical Phenomena* (Clarendon Press, Oxford, U.K., 1971).